JES Focus Issue on Electrochemical Techniques in Corrosion Science in Memory of Hugh Isaacs

Progress in Understanding Initiation of Intergranular Corrosion on AA6005 Aluminum Alloy with Low Copper Content

Shilpa Kumari,[1] Sigurd Wenner,[2] John Charles Walmsley,[2,3,a] Otto Lunder,[1,2,*] and Kemal Nisancioglu [1,*,z]

[1] *Department of Materials Science and Engineering, Norwegian University of Science and Technology, N-7491 Trondheim, Norway*
[2] *SINTEF Industry, N-7465 Trondheim, Norway*
[3] *Department of Physics, Norwegian University of Science and Technology, N-7491 Trondheim, Norway*

As part of an extensive research program to study recent, unexpected intergranular corrosion (IGC) on 6xxx series aluminum alloys (AlMgSi), this paper investigates the mechanism of initiation and early propagation of IGC on the extruded AA6005-T5 alloy with small Cu content (0.1 wt%) by use of advanced electron microscopy techniques applied for near surface characterization. Corrosion testing was restricted to the accelerated IGC test according to the standard BS ISO 11846, involving exposure to acidified chloride solution. The effect of modifying the as-received extruded surface by metallographic polishing, argon sputtering, and alkaline etching was investigated. Initiation of IGC was delayed on the as-received surface compared to the modified surface, caused by the presence of an approximately 8 nm thick crystalline oxide layer formed during extrusion. IGC initiated at the primary α-Al(Fe,Cu,Mn)Si particles for all types of surfaces. However, these particles corroded rapidly in the test solution forming a residue of Cu and Si on the exposed particle surface. This phenomenon, as well as enrichment of Cu on the Al matrix surface by dealloying, contributed increasingly to the formation of new effective cathodic sites and continuing propagation of IGC. The AlMgSiCu (Q) phase, present as primary and secondary particles, was relatively inert against both oxidation and reduction.
 [DOI: 10.1149/2.0211911jes]

Manuscript submitted March 5, 2019; revised manuscript received April 15, 2019. Published April 24, 2019. This was Paper 714 presented at the National Harbor, Maryland Meeting of the Society, October 1–5, 2017. *This paper is part of the JES Focus Issue on Electrochemical Techniques in Corrosion Science in Memory of Hugh Isaacs.*

Extruded aluminum 6xxx series (AlMgSi) alloys are characterized by a number of favorable properties, such as strength-to-weight ratio, extrudability, especially for fabrication of profiles with complex geometries, and corrosion resistance.[1] These alloys have been replacing certain steel components in the automotive industry for weight reduction without significant reduction in strength.[2] Extruded 6xxx series alloys are under consideration for subsea oil production structures for similar advantages.[3]

The usual approach for improving the mechanical properties is alloying with small amounts of Cu[4,5] and/or Si in excess of the stoichiometric ratio of the components by weight (Mg/Si $\leq$ 1.73) for the equilibrium phase Mg_2Si.[6,7] The acceptable limit for alloyed Cu in the earlier literature is 0.4%.[8] Historically, probably the first available paper regarding the possibility of IGC in acidified NaCl solution sets the Cu limit to 0.1%.[4] Both elements may cause IGC susceptibility due to unfavorable thermomechanical treatment.[5,9,10]

A recent comprehensive study of the 6005 analogue alloy, containing nominally 0.6 Mg, 0.6 Si and 0.2 Cu (in wt%), indicated significant IGC of the underaged profiles after extrusion.[11–14] A variant of the alloy with 0.02% Cu content was resistant to IGC. However, the IGC susceptibility due to 0.2% Cu was reduced and finally eliminated by artificial ageing, although overaging introduced pitting susceptibility.[12] These findings led to further research to understand the mechanism of unexpected effect of heat-treatment in reducing the danger of IGC in the presence of alloyed Cu.

Svenningsen et al. showed that IGC susceptibility was correlated with segregation of nearly continuous Cu film of a few nm in thickness along the grain boundaries in the underaged condition.[13] Furthermore, the intermetallic particles α-Al(Fe,Mn,Cu)Si and AlMgSiCu (Q-phase), which are commonly present in the alloy, were considered important as external cathodes at the initiation phase,[15] losing their significance in relation to the Cu film along the susceptible grain boundaries (internal cathodes) as IGC propagated into the metal. More recently, the role of α-phase particles as cathodes was suggested to be limited during accelerated IGC testing according to the standard BS ISO 11846, since they corroded rapidly in the acidified chloride test solution.[16] The Q-phase particles were relatively resistant to corrosion in the test solution, attributed to their high nobility in relation to the other phases in the alloy. These particles did not appear to contribute to IGC initiation, although they are expected to act as effective cathodes. Discrete Q-phase particles decorate also the bulk GBs and act as the internal cathodes for IGC propagation if the particles are connected by the Cu film. At the material surface, these particles act more as temporary barriers against IGC propagation if they are not connected to one another by the Cu film. If the film is present, the Q-phase particles delay propagation of IGC as the fissure has to propagate around the particle. Foregoing results have recently been confirmed by Kairy et al.,[17–19] by using atom probe and electrochemical measurements in addition to electron microscopy as in the earlier work, in assessing the structure of the Cu film and electrochemical properties of the relevant phases, along with extensive reviews about the role of the constituent elements, including Cu, on the properties of 6xxx-series alloys.

One can conclude from the available work that the roles of intermetallic phases, the Cu film, and the solid solution matrix alloy, especially their modification by dealloying as a result of pretreatment and testing, on the initiation and propagation mechanisms of 6xxx series alloys are not fully understood. A practical issue related to the development of Al alloys with resistance against IGC is the frequent requirement to base the studies on a highly accelerated corrosion test (BS ISO 11846). It is frequently used for the ranking of commercial alloys in research and practice, with claims about the good qualitative correspondence between the accelerated test and atmospheric field exposure.[14] The modification of the surface morphology and structure is significant due to the required pretreatment (alkaline etching) and testing (in acidified chloride solution) conditions for the accelerated test.

The purpose of this work is to contribute to further understanding of the mechanisms behind the initiation of IGC in 6xxx alloys containing of the order 0.1 wt% Cu in acidified chloride solution. In particular, it aims to investigate the effect of the test procedure on the surface microstructure and chemistry, and, thereby, on the initiation of IGC

*Electrochemical Society Member.
[a]Present address: Department of Materials Science and Metallurgy, Cambridge University, CB3 0FS Cambridge, United Kingdom.
[z]E-mail: kemaln@material.ntnu.no

Table I. Composition of alloy 6005-T5 (wt%).

Si	Fe	Cu	Mn	Mg	Al
0.64	0.21	0.14	0.16	0.57	Balance

on our benchmark alloy AA6005, by use of the available ex-situ characterization methods, and the relevance of the accelerated procedure in relation to IGC expected under actual service conditions. The propagation phase will be reported in separate papers under preparation.[20]

Experimental

Materials.—The test materials were provided by Hydro as extruded profiles prepared by the following thermomechanical processing: Billets were homogenized by heating from room temperature to 585°C in 6.5 h and held at that temperature for 2.5 h. The billets were then air cooled and extruded to 4 mm thick and 150 mm wide plate-shape profiles. Subsequent ageing was performed for 5 h at 185°C, followed by air-cooling for obtaining the T5 condition. This condition will be referred to as the as-received condition. The chemical composition of the alloy, determined by spark optical emission spectroscopy, is given in Table I. The foregoing thermomechanical process was selected for obtaining samples, which were expected to be susceptible to IGC based on our earlier work. The procedure results in the formation of a nearly continuous Cu film along the grain boundaries, which are also decorated by nanoscale Q-phase particles, connected to one another by the Cu film. Longer aging coarsens the film into discrete Q-phase particles and loss of contact between these by the absence of the Cu film, which results in increased resistance against IGC at the expense of increasing susceptibility to pitting.[11–14]

Samples were examined in the unmodified as-received condition and, also, after metallographic polishing, alkaline etching, and Ar-sputtering. The choice of pretreatment methods was based on one of the objectives to study the effect of pretreatment alkaline etching on the initiation of IGC in acidified chloride solution. In view of the fact that alkaline etching changes the surface chemistry of the alloy in addition to its morphology, metallographically polished control samples were included. Argon etching was also included since it was used in the earlier paper[16] as a mild, nonchemical surface cleaning. The as-received sample, whose surface was formed by the extrusion process and thereby preserving its original structural and chemical properties, was also included for comparison purposes and due to its importance in practice.

Polished samples were prepared by grinding with SiC papers, followed by metallographic polishing through 1 μm diamond paste. Alkaline etching was performed by immersion in 7.5 wt% NaOH solution for 3 min at 55–60°C, followed by 2 min desmutting in concentrated HNO_3 solution. Ar-sputtered samples were prepared in a Horiba Jobin-Yvon glow discharge optical emission spectrometer (GD-OES).[16] Samples were sputtered in an argon atmosphere of 600 Pa and 32 W power with an anode diameter of 4 mm. The amount of metal removed by these pretreatments from the surface was 10–15 μm for polishing and alkaline etching and 1–2 μm for Ar sputtering. Further details about the use of the GD-OES for semi-quantitative depth-profiling of the pretreated and corroded surfaces are given below under the section titled "Surface Characterization".

Corrosion testing.—Samples with exposed area of 20 × 20 mm^2 were used in corrosion testing. Accelerated corrosion testing was based on the standard BS ISO 11846 method B. The standard test requires that the samples are first alkaline etched for 1–3 min in a solution consisting of 7.5 wt% NaOH solution at 55–60°C and then desmutted in concentrated HNO_3 acid. Samples are subsequently immersed for 24 h in the acidified chloride solution (test solution) consisting of 30 g NaCl and 10 ml concentrated HCl acid (density = 1.19 g/ml) per liter of water at pH 0.95. The corrosion products are then removed by dipping in concentrated HNO_3 acid. Deviating from the standard in the present work, the surfaces of the samples were modified according to one of the methods as explained in the previous section. They were subsequently exposed to the test solution for 10 min. The as-received samples were immersed for 60 min. These modifications in the pretreatment and corrosion test were introduced in order to understand the effect of initial surface condition on IGC initiation, in particular, the induction time before initiation and the location and morphology of initiation sites.

Surface characterization.—The morphology of IGC initiation sites was investigated by use of a Zeiss Ultra field emission gun scanning electron microscope (FE-SEM). Response of the intermetallic particles and the solid solution matrix to etching and corrosion was performed semi-quantitatively by using energy dispersive X-ray spectroscopy (EDS) at an accelerating voltage of 5 kV. Quantitative analyses of the grain boundary chemistry and structure were performed by use of a JEOL JEM 2100F Transmission Electron Microscope (TEM), while the high-resolution TEM characterization of the surface oxide on the as-received sample was performed by use of a JEOL JEM ARM200F double corrected cold FEG microscope, operated at 200 kV.

The plan-view TEM foils were prepared first by light grinding of the sample surfaces, with minimum amount of material removed from the original surface on both sides for flattening. This was followed by punching of about 50 μm thick and 3 mm diameter discs. The discs were then electropolished to electron transparency in Struers TenuPol-5 unit using a solution consisting of 1/3 nitric acid + 2/3 methanol by volume. The electropolished samples were ion-milled lightly to remove the surface layer that had been exposed to the polishing bath. Cross-sectional TEM samples were prepared by the focused ion beam (FIB) lift out technique.[21] The oxide layer on the as-received sample was analyzed on cross-sectional specimens for the near-surface region. The precession-assisted crystal orientation mapping technique (PACOM) capability available on the JEM 2100F was utilized for the analysis. This is a TEM based technique, in which the diffraction pattern is acquired for a grid of points by scanning a focused probe over the area of interest. Automated indexing of the diffraction patterns allows determination of the structure and orientation of the grains down to nanometers in size.[22]

The GD-OES instrument used was a radio-frequency (RF) GD-PROFILER 2 supplied by HORIBA Jobin Yvon and operated under the conditions described above. The pressure and power specifications given above were the optimal values for the present purposes to obtain flat craters during Ar sputtering for depth profiling. The flatness of the crater bottoms was checked by use of a profilometer. The measurements were quantified for the elements present in the AA6005 alloy by using certified standards suitable for this particular alloy. The measurements were made every 5 ms during sputtering.

Electrochemical characterization.—The electrochemical tests were performed using a DC 105 Gamry potentiostat. A conventional three electrode electrochemical cell was used. 1 cm^2 area of the working electrode (sample) was exposed to the test solution by mounting the samples on special holders. Saturated calomel electrode (SCE) was used as the reference, and a platinum electrode was used as the counter electrode. Cathodic polarization tests were performed at a scan rate of 0.5 mV/s starting from the OCP. At least three replicate measurements were made for each type of sample, giving a deviation of only about 5 mV on the potential scale for the replicate measurements. The polarization curves reported below are, therefore, for selected replicates rather than averaged values.

Results

Characterization of uncorroded surfaces.—We classify uncorroded surfaces in this paper as those not yet tested by immersion in the acidified chloride solution. Morphology of the as-received surface, dominated by extrusion lines, is shown as secondary (SE) and

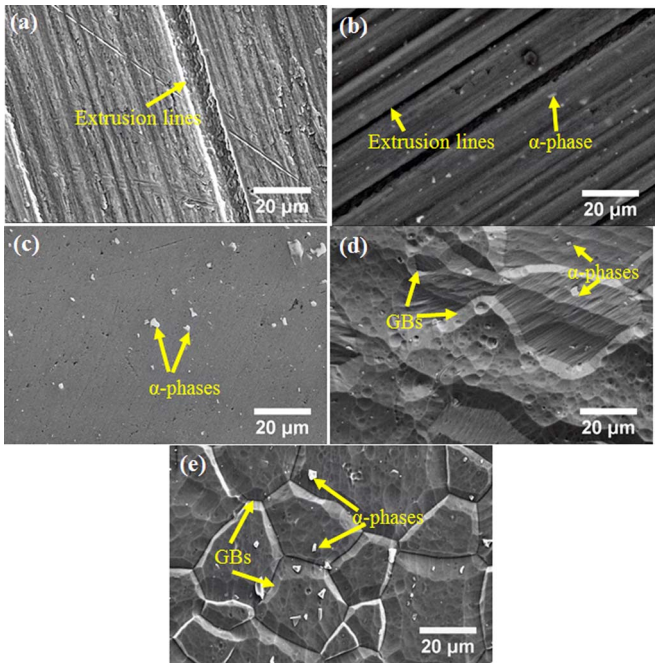

Figure 1. Surface morphologies before and after pretreatment of sample surfaces: (a) SE and (b) BSE electron images of the as-received surface obtained at electron beam accelerating voltages of 10 kV and 25 kV, respectively. SE images of (c) mechanically polished, (d) Ar-sputtered, and (e) alkaline etched surfaces.

back-scattered electron (BSE) images in Figs. 1a and 1b, respectively. Inspection of the figures indicates that many of the intermetallic particles were smeared over by a thin layer of the Al matrix alloy during extrusion. These particles become visible under the smeared layer in the BSE image (Fig. 1b), due to the greater depth of the origin of the imaging signal. Metallographic polishing exposed the intermetallic particles by removing the smeared matrix layer from the as-received surface as shown in Fig. 1c. Ar-sputtering (Fig. 1d) and alkaline etching (Fig. 1e) revealed the grain boundaries. The grain size is seen to be in the range 10–80 µm. While the intermetallic phases were largely embedded flush with the surrounding matrix surface on the polished and Ar-sputtered surfaces, they protruded from the matrix on the alkaline-etched surface.[23]

The bright particles marked with arrows in Fig. 1 are α-phase particles. Semi-quantitative EDS spot analysis of a selected α-particle on a polished sample is shown in Table II, indicating that the particles are α-Al(Mn,Fe,Cu)Si phases, where Cu appears to be enriched in the classical α-Al(Mn,Fe)Si structure.[24] EDS spot analysis of an α-phase particle on an alkaline-etched surface is also shown in Table II. Although the values for the alloying elements present in the α-phase may be affected by pick-up from the surrounding Al matrix, the composition ratios with respect to Al show reliably the increase in the amount of the noble elements due to dealloying by alkaline etching with respect to those for the polished surface (Table II).[23,25] The fact that the more noble phases etch at a smaller rate than the etching rate of the surrounding Al matrix in alkaline solution explains also the protruding morphology of these phases in Fig. 1e.[23]

Table II. EDS elemental spot analyses of selected α and Q phases on polished and alkaline etched samples of alloy 6005-T5 (at%).

	Si	Fe	Cu	Mn	Mg	Al
α phase polished	10	8.9	0.62	1.4	-	75
α phase etched	11	13	1.6	1.8	-	69
Q phase etched	10	-	1.8	-	11	75

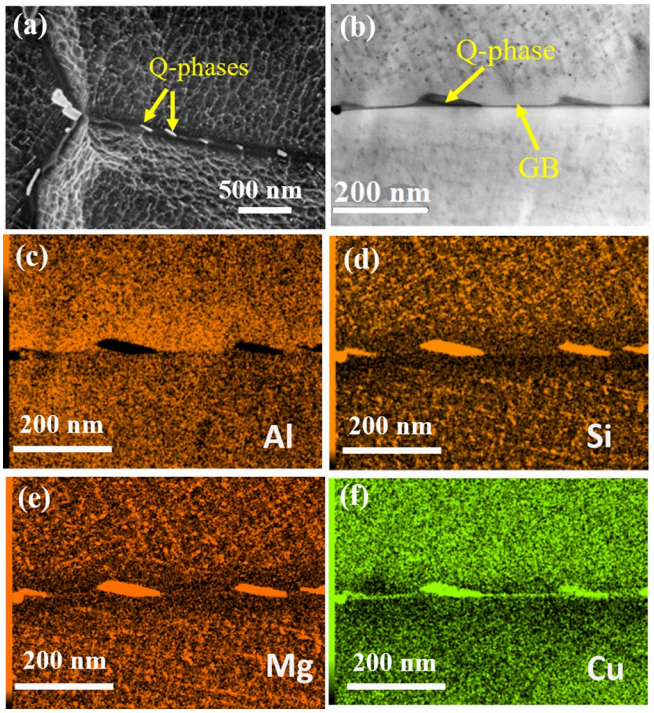

Figure 2. a) Typical distribution of Q-phase particles along a GB on the alkaline etched surface. Densely distributed, much smaller particles on the grains are the hardening precipitates. STEM image of a typical unetched GB showing (b) Q-phase particles decorating the GB and EDS maps for (c) Al, (c) Si, (d) Mg, and (e) Cu for the GB in (b). The Cu map (f) shows nearly-continuous GB nanofilm of Cu joining the adjacent Q-phase particles along the GB.

Fig. 2a shows the alkaline etched surface at a higher magnification than Fig. 1e, exhibiting the well-known scalloped morphology.[26] Semi-quantitative EDS point analysis of the rod-shaped grain-boundary phase in Fig. 2a, reveals presence of Cu, Mg and Si and absence of Fe, as shown in Table II. STEM-EDS elemental map of a similar area on an uncorroded foil (Fig. 2b) indicates depletion of aluminum in the phase with respect to the matrix (Fig. 2c), while Fig. 2d through 2f show enrichment of Si, Mg and Cu, respectively. These particles, which have their sizes in the range 100–500 nm, precipitate also in the grains and around the α-phase particles. These features identify the particles as the Q-phase, as characterized in more detail elsewhere.[14,16] STEM-EDS mapping (Fig. 2f) confirms further the presence of a nanoscale, continuous Cu-film along the grain boundaries between the Q-phase particles, as also discussed in detail earlier.[13] Corresponding depletion of these elements and increased purity of the Al matrix adjacent to the grain boundary in the EDS maps indicate the presence of a precipitate-free zone (PFZ). These results agree well with the recent literature about Cu segregation along the grain boundaries and simultaneous formation of PFZ on 6xxx series alloys with small Cu content.[14,18,19]

Oxide layer.—The air-formed oxide on aluminum alloys is normally amorphous and a few nm thick.[27] Because of its relevance to corrosion initiation in the present work, the nature of the oxide on the as-received surface was of interest, and no published literature could be found about the nature of the oxide on extruded Al surfaces. Therefore, the oxide layer was analyzed by TEM on a cross-sectional sample, prepared by FIB from the as-received condition. This showed (Figs. 3a and 3b) the presence of 8 nm thick oxide layer on the extruded surface. Only a few discrete nanocrystals could be directly observed by high-resolution TEM since their crystal lattices were randomly oriented, and only a small selection planes had their lattice planes aligned with the electron beam. By using the diffraction-based PACOM technique, the averaged diffraction pattern of the surface oxide was obtained, showing polycrystalline diffraction rings, as shown in Fig. 3c. The

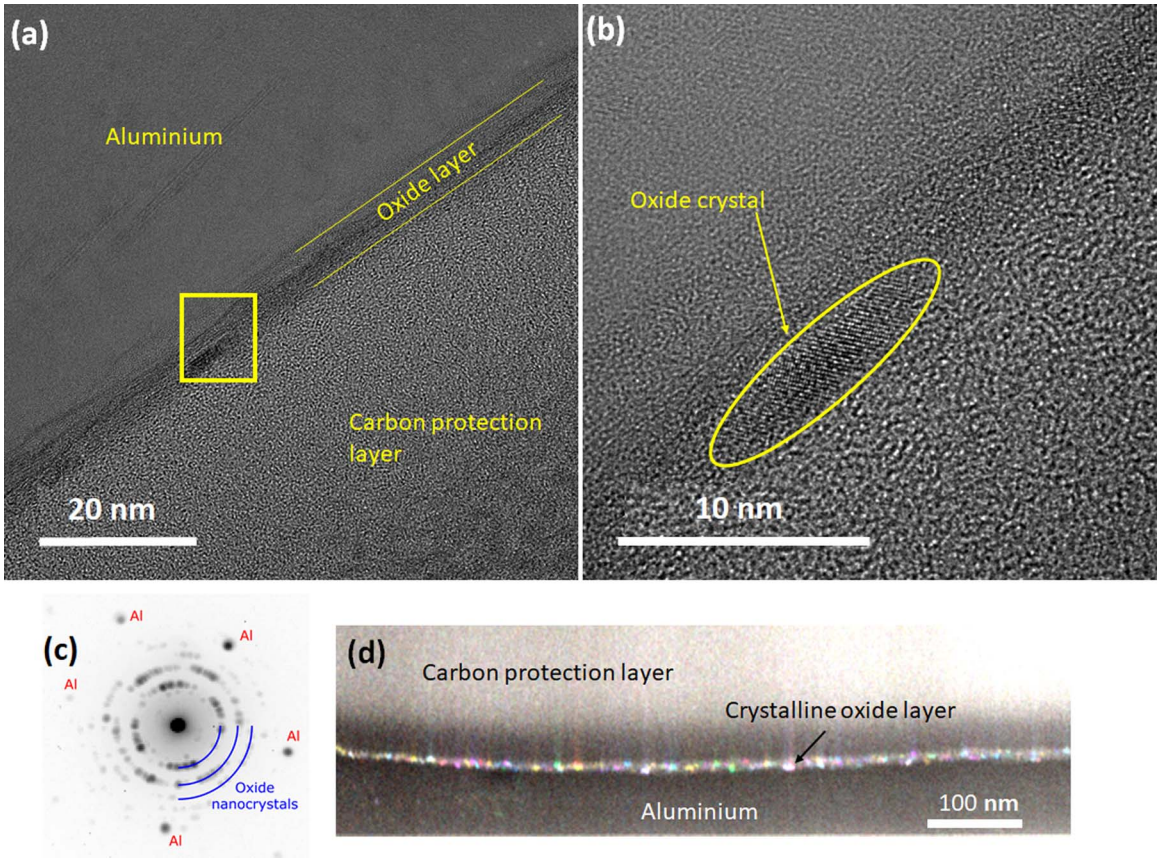

Figure 3. (a) High-resolution cross-sectional TEM image of the oxide layer on the as-received surface. (b) The area marked with a yellow square in (a) at higher magnification revealing an oxide nanocrystal. (c) Integrated diffraction pattern of the oxide from PACOM scan. (d) Virtual dark-field image of the oxide, where each color represents one spot along the diffraction rings in (c), and, therefore, one crystal orientation.

color map in Fig. 3d shows the intensity of a selection of spots belonging to the rings, indicating that the nanocrystals exist at all points along the metal surface and form a near-continuous crystalline oxide film. The crystalline oxide is formed due to the thermomechanical processing procedure used for the present specimens. Due to the similarity of their diffraction patterns, it was not possible to distinguish between the two oxides γ-Al_2O_3 and the spinel $MgAl_2O_4$, which are expected to be present.[28] Moreover, STEM-EDS mapping of the oxide layer, as shown in Fig. 4, indicated, in addition to the expected presence of Al (Fig. 4b) and O (Fig. 4c), enrichment of Mg (Fig. 4d) and minor quantities of Si (Fig. 4e) in the oxide. Therefore, the oxide layer was probably a mixture of the phases γ-Al_2O_3, $MgAl_2O_4$ and SiO_2.

GD-OES analysis.—GD-OES depth profiling was performed on the as-received surface and the surfaces modified by pretreatment and corrosion, as shown in Fig. 5. The results reported in this section were reproducible for identical replicate samples within 10% experimental error. The depth profiles are representative selected curves. However, the measured distance from the surface is much larger than expected. This is a systematic error related to surface roughness, especially on the etched and corroded surfaces.

The profiles for Al and O are shown in Figs. 5a and 5b, respectively. These profiles shift toward the left with respect to the as received surface, in the order polished, alkaline etched and corroded, indicating a slightly decreasing thickness of the surface oxide in that order.

The profiles for Cu, shown in Fig. 5c, did not change significantly from the bulk value for the as-received and polished cases. They show a significant increase, by about an order of magnitude for the alkaline etched condition, starting from about 50 nm depth below the surface. This is attributed to the enrichment of Cu as a result of selective corrosion of the more active components in the alloy and the α-phase particles, especially Al.

The Si profiles, shown in Fig. 5d, became enriched for the as-received and alkaline-etched samples by about a factor of two with respect to the bulk concentration. Polished samples show a smaller, but still significant, enrichment. The Si enrichment occurred closer to the surface than that for Cu, starting at about 25 nm depth, i.e., about half that for Cu, indicating the possibility of enriching in the oxide

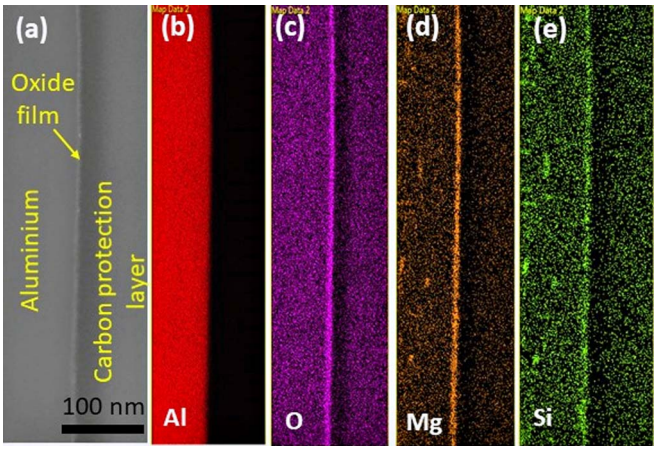

Figure 4. (a) TEM image of the cross-section of the oxide layer on an as-received sample and the EDS maps for (b) Al, (c) O, (d) Mg, and (e) Si of the image in (a).

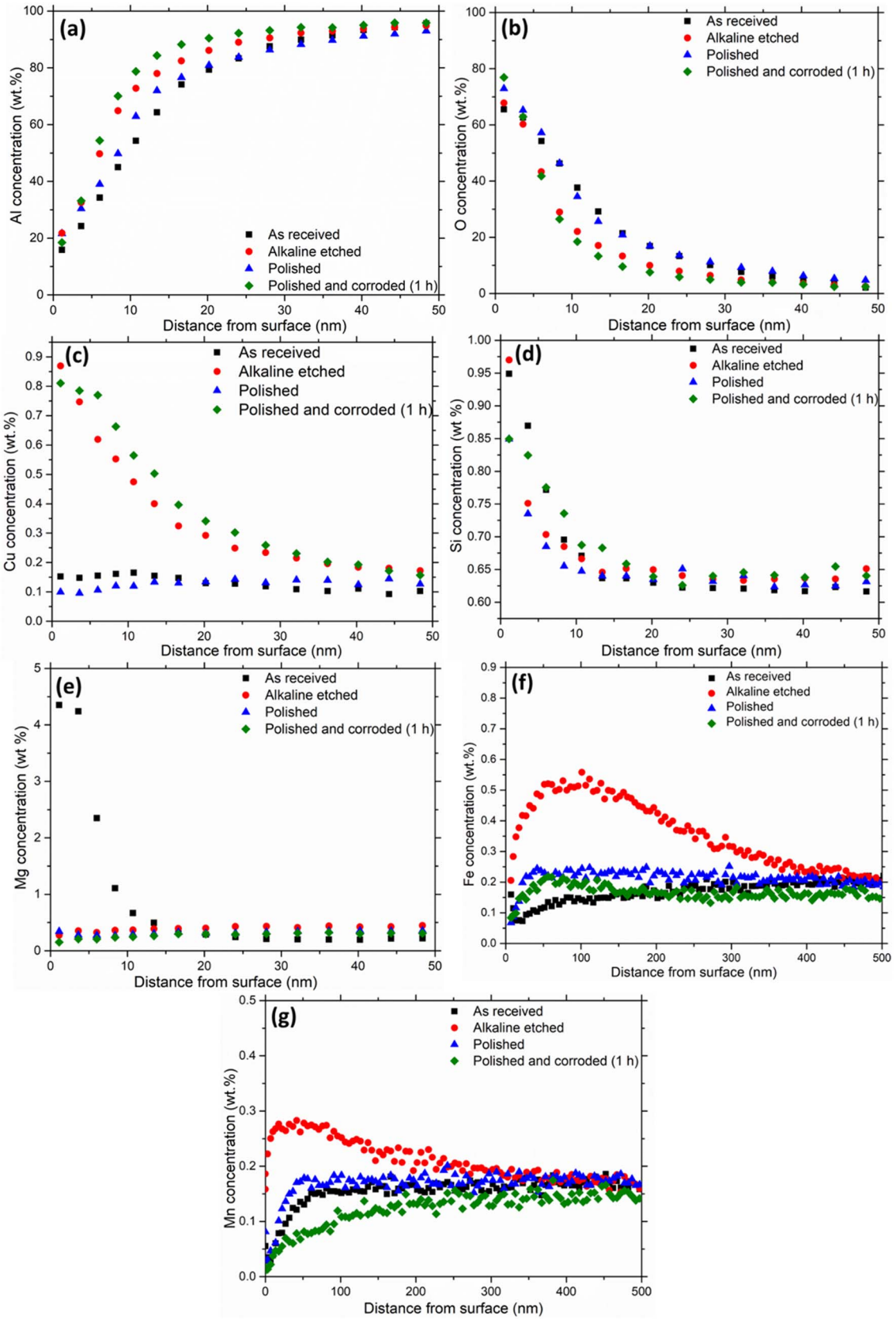

Figure 5. GD-OES elemental depth profiles of (a) Al, (b) O, (c) Cu, (d) Si, (e) Mg, (f) Fe, and (g) Mn for different pretreated surfaces.

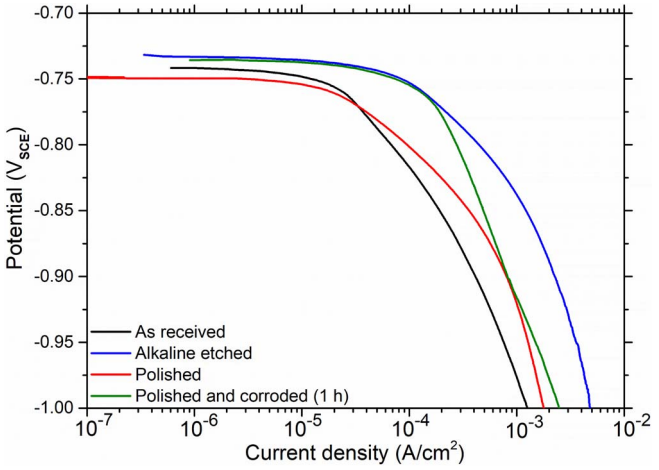

Figure 6. Cathodic polarization curves for different pretreated surfaces of AA6005 in acidified chloride solution.

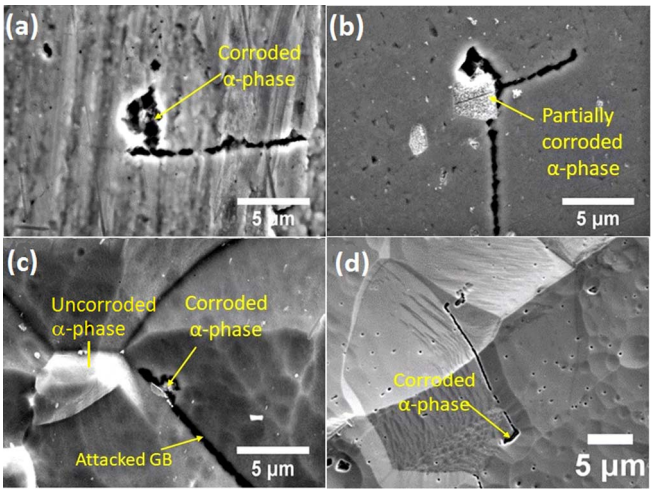

Figure 7. Examples of initiation and early growth of IGC on (a) as-received, (b) mechanically-polished, (c) alkaline-etched, and (d) Ar-sputtered surfaces. Morphologies in (a) were obtained after 1 h and the rest after 10 min exposure to the test solution.

layer, as suggested by the TEM results of the previous section for the as-received sample.

The Mg profile for the as-received sample (Fig. 5e) was similar to that of Si both in terms of magnitude and thickness (about 10 nm) of the enrichment close to the sample surface. This result verifies the oxide thickness obtained by TEM analysis above. The Mg profiles for the polished and alkaline etched surfaces did not show a significant change from the bulk value, possibly a slight depletion toward the surface. Mg oxide is expected to become enriched in the oxide as a result of alkaline etching due to its stability in alkaline solution. It probably dissolved during desmutting in nitric acid subsequent to alkaline etching.

The profiles for Fe and Mn, as shown in Figs. 5f and 5g, respectively, were somewhat similar to one another, but they were quite different from the profiles of the elements discussed above. The profiles for the two elements were quite constant at about their bulk concentrations toward the surface. They decreased closer toward the surface for the as-received and polished variants, while the profiles for the alkaline-etched variants increased to maxima, at about 0.5 wt% and 0.1 µm depth for Fe and 0.3 wt% and 0.05 µm depth for Mn, before decreasing toward the surface. The results for the elements Fe and Mn were more scattered than those for Cu, Si and Mg, and the changes occurred within a larger thickness (up to about 0.5 µm for the alkaline-etched surface) from the surface, in relation to the concentrations of the other elements. These differences are related to the fact that Fe and Mn are largely incorporated in the α-phase particles, which are scattered in terms of size and position at the surface, while the other elements are segregated within a more uniform and thinner layer closer to the surface either in the oxide or solid-solution aluminum matrix.

Cathodic polarization.—Cathodic polarization curves for different pretreated surfaces, obtained in acidified chloride solution, indicate that the alkaline etched surface had the highest cathodic activity, followed by the corroded surface, as shown in Fig. 6. Increase in the cathodic activity by alkaline etching is attributed to the exposure of a larger number density of α-phase particles and their further enrichment with the nobler elements of Fe, Mn and Cu. The corroded sample had a higher cathodic activity than the polished surface, also attributable to the enrichment of Cu, as indicated by the GD-OES data in Fig. 5c. The polished surface appears to be slightly more cathodic than the as-received surface, possibly due to a larger area of exposed α-phase particles at the outset of the polarization run due to removal of the oxide and smeared matrix layers formed during extrusion discussed earlier in the paper.

The anodic behavior of the surface types in question (not shown) could not be distinguished by anodic polarization due to poor reproducibility resulting from pitting in acidified chloride solution, and also because of the fact that pitting corrosion is determined more by the properties of the bulk material than the surface. Convergence of the cathodic polarization curves in Fig. 6 toward the corrosion potential, which is not too different for the surface types at the outset within the reproducibility limits, indicates such behavior.

Corrosion morphology.—*IGC initiation.*—In order to examine the initiation of IGC on as-received and pretreated surfaces, immersion in acidified chloride solution was performed for different time periods. Fig. 7a shows typical IGC morphology on the as-received surface after 1 h of exposure. The figure suggests that IGC initiated locally at an α-phase particle. A similar conclusion can be drawn for IGC initiation on the pretreated surfaces, metallographically polished (Fig. 7b), alkaline etched (Fig. 7c), and Ar sputtered (Fig. 7d), verifying the results of earlier introductory work.[16] However, IGC initiated faster on the pretreated surfaces than on the as-received surface, i.e., after 10–15 min of immersion on pretreated surfaces, as opposed to about 1 h on the as-received surface. Fig. 7c, shows α-phase particles on the grain boundaries without any IGC initiation in their immediate vicinity, indicating that not all α-phase particles on the grain boundaries were necessarily initiation sites for IGC.

Corrosion of intermetallic phases.—The α-phase itself corroded during immersion in acidified chloride solution, in agreement with the earlier study,[16] as shown in Figs. 7a–7d and Fig. 8, leaving a Cu-rich residue, as indicated by the EDS map for Cu shown as inset to Fig. 8.

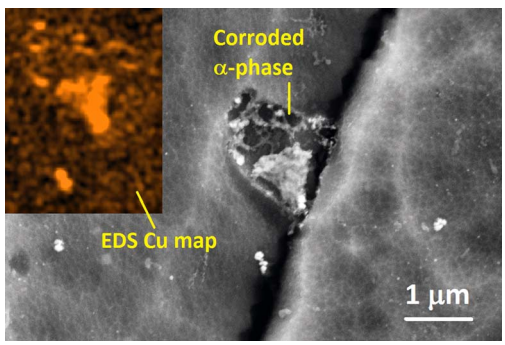

Figure 8. SEM image of corroded α-phase on originally alkaline etched surface after 15 min corrosion in the acidified chloride test solution. Inset shows EDS Cu map of the area of the corroded α-phase.

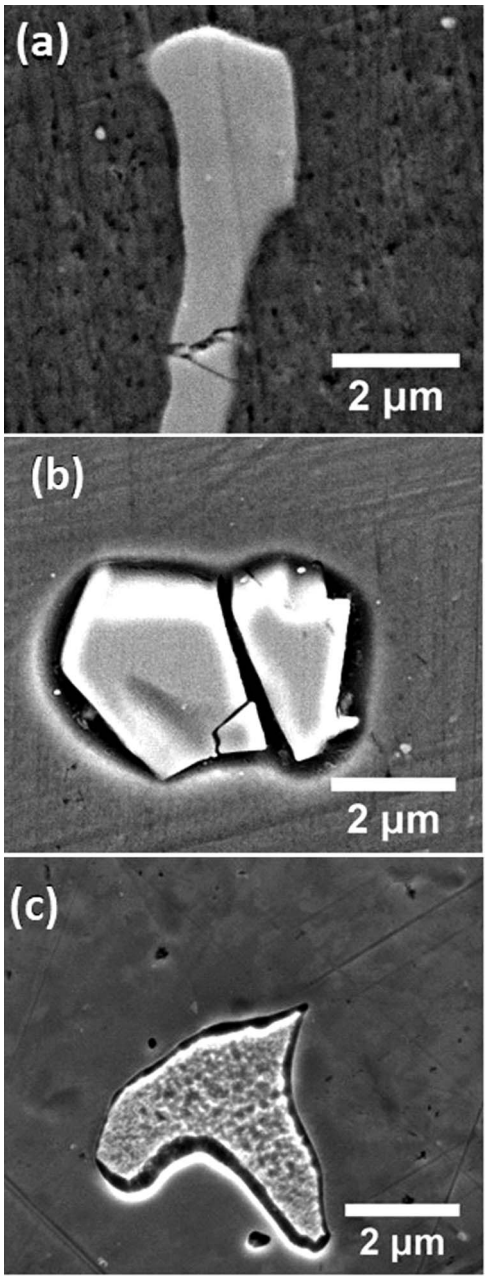

Figure 9. Morphology of α-phases on polished surfaces (a) before corrosion and (b) after 5 min and (c) 10 min corrosion in the test solution.

Although not shown, no detectable Fe and Mn remained, and a trace amount of Si could be detected in the α-phase particles after 15 min exposure to the acidified chloride solution.

Fig. 9 shows a closer study of different stages of corrosion on α-phase particles, selected in the bulk of grains away from the grain boundaries and, therefore, not affected by IGC in the acidified chloride solution. Fig. 9a shows an uncorroded particle on a polished sample surface. Corrosion of the matrix around the particles at the outset formed a ditch as shown in Fig. 9b, indicating that the α-phase behaved as the cathode of the microgalvanic couple, as is well known from earlier studies.[23] However, the α-phase also started to corrode, as discussed above, leaving a porous dealloyed layer, as shown in Fig. 9c.

The Q-phase was observed to be relatively inert in relation to the α-phase. Fig. 10 shows another example of uncorroded Q-phase particles at the bottom of a pit formed by corrosion of an α-phase, initially located at a triple grain-boundary junction. There is no obvious sign of

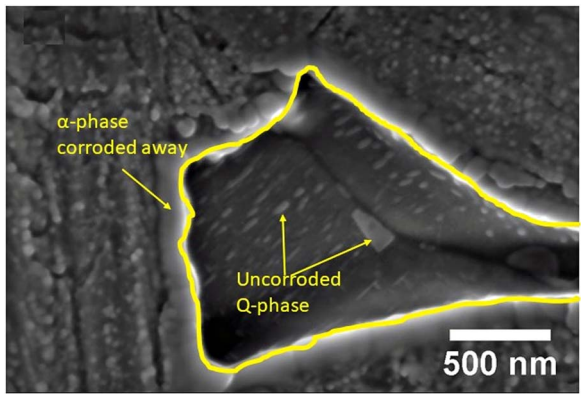

Figure 10. Uncorroded Q-phase particles revealed at the bottom of the pit formed by corrosion of an α-phase on a triple point grain-boundary after 20 min exposure to the test solution.

IGC initiation and propagation related to the Q-phase particles at the grain boundaries exposed by corrosion of the α-phase. Fig. 11a shows IGC attack along the grain boundaries except stretches without any attack or slight etching probably due to the presence of PFZ. A higher magnification micrograph of the unattacked grain boundary, shown in Fig. 11b, reveals that Q-phase particles are decorated, and possibly acting temporarily as a physical barrier against IGC, along the stretch.

Discussion

The present work confirms and supplements earlier results[16] with new evidence that IGC initiates at the α-phase particles precipitated along the grain boundaries on alloy AA6005 in acidified chloride solution, and that the Q-phase behaves relatively inert during the initiation

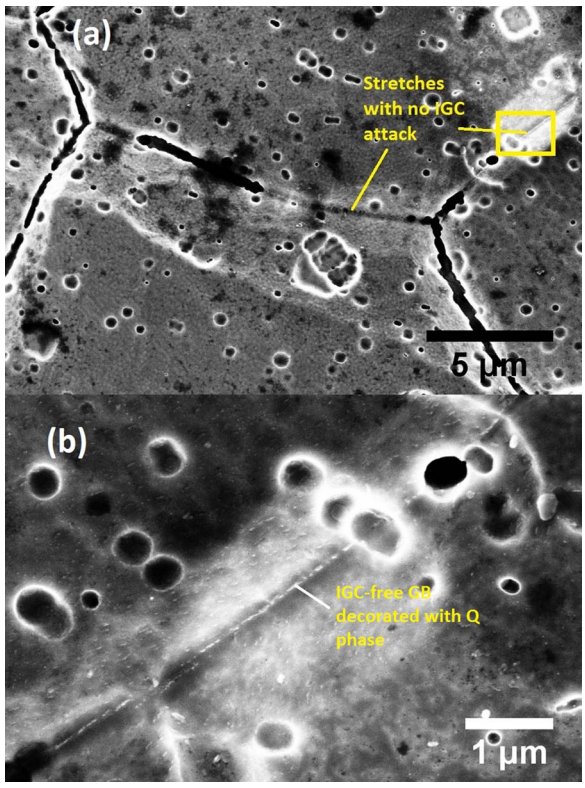

Figure 11. (a) SEM image of a string of Q-phase particles along the grain boundary after 24 h corrosion in the test solution. (b) Area marked with yellow square in (a) at a higher magnification.

phase. Moreover, corrosion susceptibility of the α-phase itself to the acidified chloride solution is confirmed, showing in addition that all components of the phase, except Cu and possibly Si, corrode selectively. The surface morphologies developing during the initiation stage indicate further that the α-phase acts as a significant cathode in providing the cathodic current needed for its self-corrosion, as well as the current needed for microgalvanic corrosion of the matrix around itself (Fig. 9b). The α-phase particles precipitated along the grain boundaries, provide both the initiation site, probably as pits formed by corrosion of the α-phase particles or the ditches developing between the α-particles and the matrix, and the cathodic current needed for the transformation of the attack into IGC when the adjacent grain boundary has the necessary conditions (Cu film as the internal cathode) to support such corrosion. The results demonstrate, moreover, that the α-phase particles, which are precipitated in the grains, also participate in the process. The remnants in the form of metallic Cu, as long as they remain attached to the surface, are also expected to continue to function as effective external cathodes. The α-phase particles are eventually removed by corrosion, possibly also by detachment due to corrosion of the matrix alloy adjacent to the particles. However, fresh particles are exposed as a result of uniform etching of the surface in the acidified chloride solution, and the above process continues during propagation. At the same time, Cu is enriched more uniformly on the matrix as a fresh external cathode, as will be discussed further below. Therefore, the external cathodes appear to have an important role, at least, in the initiation of IGC for the present alloy-environment combination.

The Q-phase particles decorate nearly all GBs and probably contribute as cathodes if the GB is susceptible to IGC. For IGC susceptibility, however, connection of these phases by the nearly continuous Cu GB film is required as demonstrated by our earlier work.[11–15] Without the film, IGC fissures cannot propagate from one GB particle to the next, and the GB becomes immune to IGC. Further discussion of the fissure propagation mechanism and the role of the intermetallic phases in it are outside the present scope.

Different pretreatments such as metallographic polishing, alkaline etching, and Ar-sputtering were selected to explore the difference in the initiation of IGC due to changes in the surface morphology. The difference in the induction time for initiation between the pretreated surfaces, involving mechanical, chemical or physical material removal, was not significant, but quite faster than the initiation on the as-received surface. This is attributed to the presence of the crystalline oxide and smeared metal layer on the as-received sample after extrusion, both providing extra resistance against the initiation of localized corrosion. The smeared matrix layer also seems to cover the cathodic intermetallic particles.[29] All selected pretreatment methods remove both the crystalline oxide layer and smeared metal, leading to the formation of less protective air-formed oxide and exposure of the detrimental cathodic intermetallic particles at the surface.

Formation of crystalline (γ-Al_2O_3) oxide as a result of exposure of Al alloys to high temperatures, such as 500–600°C as in the extrusion of the present samples, is a well-known phenomenon.[30,31] It has also been shown that mixed crystalline oxides, such as the type discussed in this paper, can form on multicomponent alloys.[28] The oxide crystals grow from the surface into the metal by ingress of oxygen through the gaps between the crystals. Heat treatment in air limits the thickness of the crystalline layer to about 50 nm, which is attained, after about 10 min exposure to 600°C. The size of the crystals formed is the same as the film thickness since the thickness is limited to a single layer, as can be deduced from Fig. 3d. The properties of the oxide formed by extrusion, in which the surface is exposed to temperatures of similar magnitude, but for a significantly shorter period of time, appear to be identical to those grown to steady-state thickness except for the crystal size and, therefore, the film thickness. The added presence of magnesium in the form of MgO and/or the spinel $MgAl_2O_4$ is also known to improve the protection of the oxide against localized corrosion in chloride solution.[28,32]

Initiation of IGC was not observed at other possible sites, such as the Q-phase, besides the α-phase. However, the results showed that not all α-phase particles along the grain boundaries act as initiation sites for IGC. This may be related to the level of Cu in individual particles and absence of the Cu-rich grain-boundary film at that site. The composition windows of the constituent elements Fe, Mn and Cu are quite large for the stability of the α-phase, allowing significant variations of these elements from one particle to another in a given sample.[8] The effectiveness of the cathodic behavior is expected to increase with increasing concentration of Cu in the phase. Initiation is a stochastic process, and the sites, at which IGC initiates first, may cathodically protect against initiation at certain other sites. A grain boundary with Cu-film may not exist adjacent to all α-phase particles to initiate sustained IGC. Smaller Q-phase particles precipitate amply around the larger α-phase particles because the latter appears to act as a good nucleation site. However, the Q-phase particles do not appear to contribute much to the initiation of IGC. The presence of the Cu film along the grain boundary with PFZ appears to be necessary for initiation and propagation of IGC on the particular material investigated.[16,19]

GD-OES profiles for Cu (Fig. 5c) indicate that Cu, the noblest component in the alloy, is enriched as a result of chemical processing of the surface, in the present case both in alkaline and acid environments. The same is the case for Si (Fig. 5d). Si is enriched also on the as-received samples. This is shown to occur in the oxide (Fig. 4e). Fe and Mn are enriched by alkaline etching, as well known from earlier studies,[23] and removed by corrosion in the acidified chloride solution. In the case of these two elements, enrichment in alkaline solution occurs locally on the α-phase particles, since nearly all Fe and Mn in the alloy are present in the form of α-phase. For the present temper (T5) of the AA6005 specimens, most Cu and Mg are expected to precipitate as much smaller and more uniformly distributed secondary hardening phases (Mg_2Si, Q and their precursors)[6] relative to the coarser and randomly distributed α-phase particles.

The difference in the depth profiles for Fe and Mn in relation to those of Cu and Si indicates that the latter two segregate much closer to the sample surface. This is verified by the fact that Si is segregated mainly in the oxide on the as-received sample (Figs. 4e and 5d). The shape of the Fe and Mn profiles, in terms of formation of maxima near the surface in alkaline solution and larger scatter than the curves for Cu and Si, suggest that the typical form of segregation of these elements is in coarse and randomly distributed α-particles. Smaller scatter in the profiles for Cu and Si indicates for these elements that the GD-OES data are more representative of segregation in the secondary hardening phases (Q-phase) and/or their presence in solid solution with the aluminum matrix rather than in the form of primary particles. This indicates that corrosion of the present alloy of interest causes relatively uniform enrichment of the noble element Cu at the surface, while the elements Fe and Mn, also nobler than Al, are depleted at the surface by exposure to the acidified chloride solution. Enrichment of Cu at the surface, both locally by dealloying of the α-phase and more uniformly over the entire exposed surface by dealloying of the matrix, strengthens the role of a dominating external cathode both in the initiation and propagation phases of IGC.

Segregation of Si from solid solution into the oxide during extrusion and from the MgSi-rich hardening phases during alkaline and, possibly, acid etching is expected to occur in a manner similar to that of Cu discussed above. However, it is expected to be in the form of a Si oxide, shown to be relatively inert as a cathode on Al.[15] The GD-OES data (Fig. 5e) also verify the TEM results (Fig. 4d) that Mg is included in the crystalline oxide formed during extrusion.

These are factors, which are expected to contribute to the resistance and passivity of the oxide on the as-received surface, as observed presently in terms of increased induction time for initiation of IGC. Removal of the oxide layer, together with the surface metal smeared over the intermetallic particles, by surface pretreatment is thus understood as an important accelerating factor in the standard BS ISO 11846 test for IGC corrosion. Moreover, significant acceleration of IGC initiation is expected on the alkaline-etched surface by the enrichment of the noble elements as cathodes before exposure to the acidified

chloride solution. Enrichment of Cu by dealloying in the acidified chloride solution is an added factor.

The accelerated test used in this work is commonly applied both in industrial practice and in research. It seems to be successful in predicting if the 6xxx-series aluminum alloy is susceptible to IGC or not. The extent to which it realistically represents the IGC of structural elements of 6xxx alloys due to atmospheric conditions deserves further evaluation.

Investigation of initiation of localized corrosion on wrought aluminum alloys and their worked surfaces often brings to the fore the possible significance of an "altered surface layer" (ASL) formed during thermomechanical processing of the aluminum alloy, such as by hot and cold rolling, machining, and abrasion.[33] ASLs are not known to occur on extruded surfaces. Although outside the scope of the present paper, the smeared metallic layer observed to form by extrusion of our 6005 samples, may call for a discussion of existence of such layers on these samples, based on the results presented in this paper. It is widely documented, as reviewed in Ref. 33, that the large GB area per volume of ASLs, in relation to that observed in the bulk GBs, formed by the thermomechanical treatment, are ideal sites for ample precipitation of nanosize Al-base intermetallic particles, such as the α and Q-phases, and segregation of nearly continuous films rich in trace elements, such as Pb[35] and Sn,[36] from Group IIIA - VA elements. These precipitates and segregations activate the surface, either cathodically or anodically, respectively, and such behavior can be utilized as an indirect method to detect the presence of ASLs. GD-OES is also a well-suited method for investigation of such layers, assuming that the layer is contaminated by the activating elements/compounds.[34]

Present GD-OES data for the as-received surface (Fig. 5), do not indicate any enrichment of the transition elements Cu, Mn and Fe near the surface, where the concentrations of the elements are nearly the same as their bulk values within the stated error limits. The same is true for the polished surfaces. The only element enriched in this case is Mg in the oxide (Fig. 5e), as expected and discussed above. Anodic polarization curves are not affected by surface pretreatment, ruling out the anodic activating effect of any Group IIIA - VA elements. Chemical (acid or alkaline) etching is the only way to modify the surface composition and, thereby, the electrochemical behavior of the extruded surface, and it happens by the enrichment of the noble elements by dealloying rather than the influence of an ASL. High-resolution TEM results (Fig. 3) do not show any sign of ASL either. Therefore, the present results do not indicate any evidence of ASL to have an impact on the initiation phase of IGC. However, the methods used in reaching this conclusion, except for the TEM results, are indirect. Alignment of the electron beam with respect to the oxide-metal interface, which is necessary for the observation of such layers, may have to be improved. The use of other advanced methods, such as atom-probe analysis, may be needed for a more definite conclusion in future work, which has to be more focused toward unambiguous detection of ASLs.

Conclusions

1. For all surface types (as-received and modified by alkaline etching, Ar-sputtering, and mechanical polishing) of alloy AA6005, IGC in acidified chloride solution was initiated at the α-Al(Fe,Cu,Mn)Si particles. Initiation actually occurs in pits formed by rapid corrosion of the α-phase particles in the acidified NaCl test solution.
2. These particles acted also as effective cathodes during the initiation phase despite their simultaneous self-corrosion. The Cu-rich remnants of the α-phase and Cu enrichment of the surface due to dealloying of the Al matrix alloy became significant as external cathodes for IGC initiation and propagation.
3. No sign of IGC initiation was detected at the Q-phase particles. Q-phase was passive in relation to the α-phase as the external cathode during the initiation of IGC. Neither was it affected significantly, in relation to the α-phase, by exposure to the test solution. The most significant role of the phase in IGC of the AA6005 alloy was as an inert barrier against initiation of IGC fissures and early stage of their growth.
4. As-received surface was covered by an 8 nm thick mixed oxide consisting of γ-Al_2O_3 and the spinel $AlMg_2O_4$. Due to this protective crystalline layer, along with a smeared surface layer of deformed solid-solution aluminum matrix, which tended to cover the cathoically-active surface, the induction time for initiation of IGC was longer (1 h) on the as-received surface than for the pretreated surface (10–15 min).
5. The present conclusions about initiation of IGC are restricted to BS ISO 11846 accelerated corrosion test, which is widely used in research and industrial quality control. The environment and procedures used are very different from those applied for long-term immersion and atmospheric corrosion tests, and the results have to be used with care for ranking purposes. Extensive modifications of the surface morphology and chemistry caused by pretreatment and during exposure to the acidified chloride environment do not justify any attempts for lifetime prediction.

Acknowledgments

This work was performed as part of the Norwegian national project entitled, *Fundamentals of Intergranular Corrosion in Aluminum Alloys (FICAL)*, supported by The Research Council of Norway (contract no. 247598), Hydro, Gränges, Benteler Automotive Raufoss, and Steertec Raufoss. The STEM work was performed under the auspices and infrastructure of the Norwegian Transmission Electron Microscopy Center (NORTEM) supported by The Research Council of Norway, contract no. 197405.

ORCID

Kemal Nisancioglu https://orcid.org/0000-0003-3712-8238

References

1. D. G. Altenpohl, *Aluminum viewed from within: an introduction into the metallurgy of aluminum fabrication*, Aluminum-Verlag, Düsseldorf (1982).
2. H. Helms and U. Lambrecht, *Energy savings by light-weighting. Final report for the International Aluminium Institute*, Institute for Energy and Environmental Research. Heidelberg, 2003.
3. S. Røstbø, H. Solli, O. Lunder, and K. Nisancioglu, "Cathodic Protection against Galvanic-Crevice Corrosion of Steel-Aluminium Couples in Sea Water," EUROCORR 2017, European Federation of Corrosion Event No. 417, September 3 - 7, 2017, Prague, Czech Republic
4. H. Hug, *Aluminium*, **23**(1), 33 (1941).
5. K. Yamaguchi and K. Tohma, *J. Japan Inst. Light Metals*, **47**, 285 (1997).
6. A. K. Gupta and D. J. Lloyd, *Mat. Sci. Eng. A*, **316**, 11 (2001).
7. D. J. Chakrabarti and D. E. Laughlin, *Prog. Mater. Sci.*, **49**, 389 (2004).
8. L. F. Mondolfo, *Aluminum Alloys: Structure and Properties*, Butterworths, London (1976).
9. R. Dif, B. Bes, J. C. Ehrström, C. Sigli, J. T. Warner, P. Lassince, and H. Ribes, *Mater. Sci. Forum*, **331–337**, 1613 (2000).
10. V. Guillaumin and G. Mankowski, *Corrosion*, **56**, 12 (2000).
11. G. Svenningsen, M. H. Larsen, J. H. Nordlien, and K. Nisancioglu, *Corr. Sci.*, **48**, 258 (2006).
12. G. Svenningsen, M. H. Larsen, J. H. Nordlien, and K. Nisancioglu, *Corr. Sci.*, **48**, 3969 (2006).
13. G. Svenningsen, M. H. Larsen, J. C. Walmsley, J. H. Nordlien, and K. Nisancioglu, *Corr. Sci.*, **48**, 1528 (2006).
14. G. Svenningsen, J. E. Lein, A. Bjørgum, J. H. Nordlien, Y. Yu, and K. Nisancioglu, *Corr. Sci.*, **48**, 226 (2006).
15. M. H. Larsen, J. C. Walmsley, O. Lunder, and K. Nisancioglu, *J. Electrochem. Soc.*, **157** C61 (2010).
16. K. Shimizu and K. Nisancioglu, *ECS Electrochem. Lett.*, **3**, C29 (2014).
17. S. K. Kairy, P. A. Rometsch, K. Diao, J. F. Nie, C. H. J. Davies, and N. Birbilis, *Electrochim. Acta*, **190**, 92 (2016).
18. S. K. Kairy, T. Alam, P. A. Rometsch, C. H. J. Davies, R. Banerjee, and N. Birbilis, *Metall. Mater. Trans. A*, **47a**, 985 (2016).
19. S. K. Kairy, P. A. Rometsch, C. H. J. Davies, and N. Birbilis, *Corrosion*, **73**, 87 (2016).
20. S. Kumari, "Initiation and Propagation of Intergranular Corrosion on AA6005 Aluminium Alloy," *Ph.D. Thesis*, Norwegian University of Science and Technology, Trondheim, Norway (2018).
21. R. M. Langford and C. Clinton, *Micron*, **35**, 607 (2004).
22. D. Viladot, M. Véron, M. Gemmi, F. Peiró, J. Portillo, S. Estradé, J. Mendoza, N. Llorca-Isern, and S. Nicolopoulos, *J. Microsc.*, **252**, 23 (2013).

23. O. Lunder and K. Nisancioglu, *Corrosion*, **44**, 414 (1988).
24. P. Orozco-Gonzalez, M. Castro-Roman, J. López-Rueda, A. Hernández-Rodríguez, R. Muñiz-Valdez, S. Luna-Álvarez, and C. Ortiz-Cuellar, *Rev. Metal. Madrid*, **47**, 453 (2011).
25. K. Nisancioglu, *J. Electrochem. Soc.*, **137**, 69 (1990).
26. A. Abouarkoup, G. Thompson, X. Zhou, and G. Scamans, *Journal of Minerals and Materials Characterization and Engineering*, **4**, 364 (2016).
27. N. H. Giskeødegård, O. Hunderi, and K. Nisancioglu, *J. Solid State Electrochem.*, **19**, 3473 (2015).
28. Y. Yu, Ø. Sævik, J. H. Nordlien, and K. Nisancioglu, *J. Electrochem. Soc.*, **152**, B327 (2005).
29. T. Sheppard, *Extrusion of Aluminum Alloys*, Springer-Science+Business Media, Dordrecht (2013).
30. J. I. Eldridge, R. J. Hussey, D. F. Mitchell, and M. J. Graham, *Oxid. Met.*, **30**, 301 (1988).
31. K. Shimizu, R. C. Furneaux, G. E. Thompson, G. C. Wood, A. Gotoh, and K. Kobayashi, *Oxid. Met.*, **35**, 427 (1991).
32. D. J. Field, G. M. Scamans, and E. P. Butler, *Metall. Trans. A*, **18**, 463 (1987).
33. S.-S. Wang, F. Yang, and G. S. Frankel, *J. Electrochem. Soc*, **164**, C317 (2017).
34. Y. W. Keuong, J. H. Nordlien, S. Ono, and K. Nisancioglu, *J. Electrochem. Soc.*, **150**, B547 (2003).
35. Anawati, B. Graver, H. Nordmark, Z. Zhao, G. S. Frankel, J. C. Walmsley, and K. Nisancioglu, **157**, C313 (2010).
36. J. Tan and K. Nisancioglu, *Corr. Sci.*, **76**, 219 (2013).